

Journal of Biomedical Optics

BiomedicalOptics.SPIEDigitalLibrary.org

Mapping of cutaneous melanoma by femtosecond laser-induced breakdown spectroscopy

Youngmin Moon
Jung Hyun Han
Jang-hee Choi
Sungho Shin
Yong-Chul Kim
Sungho Jeong

SPIE.

Youngmin Moon, Jung Hyun Han, Jang-hee Choi, Sungho Shin, Yong-Chul Kim, Sungho Jeong, "Mapping of cutaneous melanoma by femtosecond laser-induced breakdown spectroscopy," *J. Biomed. Opt.* **24**(3), 031011 (2018), doi: 10.1117/1.JBO.24.3.031011.

Mapping of cutaneous melanoma by femtosecond laser-induced breakdown spectroscopy

Youngmin Moon,^{a,†} Jung Hyun Han,^{b,c,†} Jang-hee Choi,^a Sungho Shin,^a Yong-Chul Kim,^b and Sungho Jeong^{a,*}

^aGwangju Institute of Science and Technology, School of Mechanical Engineering, Gwangju, Republic of Korea

^bGwangju Institute of Science and Technology, School of Life sciences, Gwangju, Republic of Korea

^cSaint John of God Hospital, Department of Dermatology, Gwangju, Republic of Korea

Abstract. Surgical excision (Mohs micrographic surgery) is the standard procedure to treat a melanoma, in which an *in situ* histologic examination of sectioned skin is carried out repeatedly until no cancer cells are detected. The possibility to identify melanoma from the surrounding skin by femtosecond laser-induced breakdown spectroscopy (fs-LIBS) is investigated. For experiments, melanoma induced on a hairless mouse by injection of B16/F10 murine melanoma cell was sampled in the form of frozen tissue sections as in Mohs surgery and analyzed by fs-LIBS ($\lambda = 1030$ nm, $\tau = 550$ fs). For analysis, the magnesium signal normalized by carbon intensity was utilized to construct an intensity map around the cancer, including both melanoma and surrounding dermis. The intensity map showed a close match to the optically observed morphological and histological features near the cancer region. The results showed that when incorporated into the existing micrographic surgery procedure, fs-LIBS could be a useful tool for histopathologic interpretation of skin cancer possibly with significant reduction of histologic examination time. © The Authors. Published by SPIE under a Creative Commons Attribution 4.0 Unported License. Distribution or reproduction of this work in whole or in part requires full attribution of the original publication, including its DOI. [DOI: 10.1117/1.JBO.24.3.031011]

Keywords: laser-induced breakdown spectroscopy; melanoma; medical and biological imaging; mapping; histology.

Paper 180386SSR received Jun. 27, 2018; accepted for publication Sep. 27, 2018; published online Oct. 12, 2018.

1 Introduction

Melanoma is acknowledged as the most dangerous form of skin cancer, accounting for 90% of the deaths associated with cutaneous cancers.¹ According to a recent report,¹ the incidence of melanoma is increasing worldwide with the regional incidence rate of up to 10 to 20, 20 to 30, and 50 to 60 per 100,000 populations in Europe, USA, and Australia, respectively. The standard treatment of an operable melanoma involves surgical excision with a safety margin. The safety margin is required in order to completely remove not only the primary cancer but also melanoma cells that might have spread into the surrounding skin.² The determination of a proper safety margin is critical during surgical treatment because a too-large safety margin leaves functionally and cosmetically poor outcome, whereas a too-small safety margin risks incomplete removal of cancer or cancer cells. For the determination of safety margin, Mohs micrographic surgery is widely adopted in dermatology, in which the process of cancer excision and histologic examination is repeated until no cancer cells are found from the excised layer.³ An accurate interpretation of the histologic examination of excised layer during the surgery is critical. One of the shortcomings of the Mohs procedure is the prolonged operation time due to repeated histology test during the surgery, which increases the risk of complications such as wound infection.⁴ Thus an alternative or supporting technique to accurately and rapidly determine the cancer region and appropriate safety margin is highly desired.

Laser-induced breakdown spectroscopy (LIBS) is a technique, in which the concentrations and distributions of

constituent elements of a sample are analyzed by measuring the emission from laser produced plasma. LIBS measurement can be completed in a short time (on the order of seconds or shorter) and performed in air with little or no sample preparation. Owing to the speed and high-spatial resolution achievable with LIBS, the application of LIBS for the classification of biological samples, such as liver,⁵ breast and colorectal tissues,⁶ and nerve and fat of pig heads,⁷ carious teeth⁸ has been investigated by many researchers, demonstrating the potential as a fast classification method. Although LIBS is a relatively new technique, other spectroscopic methods have been widely investigated for detection and imaging of skin cancer, such as infrared spectroscopy⁹ or Raman spectroscopy,¹⁰ which provides the molecular information of a sample. On the contrary to these molecular spectra-based techniques, LIBS provides the atomic spectra of the constituent elements. Thus it may be used independently or complementarily with a molecular spectroscopic method for the diagnosis of skin cancer. For instance, a recent study reported the combination of LIBS and Raman spectroscopy for the classification of bacteria.¹¹ For the case of melanoma, we reported in our recent study that melanoma and surrounding dermis could be distinguished by LIBS with high sensitivity using Mg and Ca emission peaks as the biomarkers.¹² Although it was an early stage of research yet, this study confirmed that LIBS can be an effective method to identify melanoma from normal tissue.

Although the spectral information itself in our previous study¹² is useful in determining the pathological state of the tissue, an elemental mapping image based on LIBS spectral intensity can provide a direct information to assess the skin cancer region and required margin during a surgical excision. In the case of Mohs micrographics surgery, LIBS elemental mapping may be applied to a sectioned tissue to rapidly create

*Address all correspondence to: Sungho Jeong, E-mail: shjeong@gist.ac.kr

†Co-first authors with equal contribution.

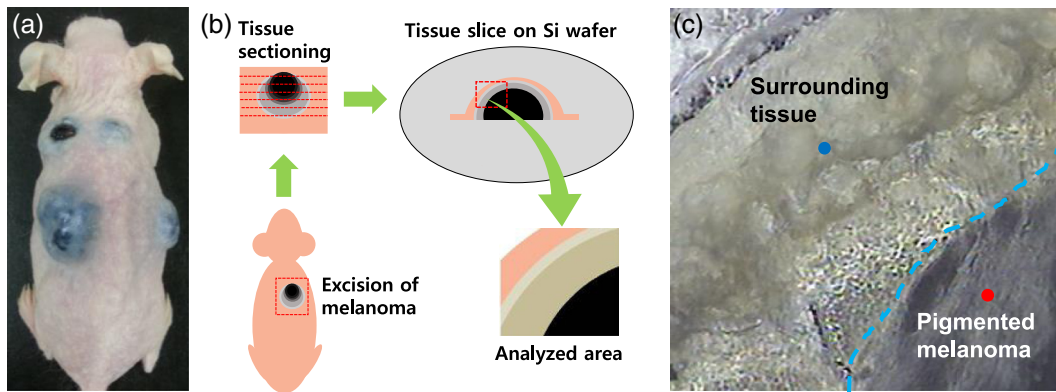


Fig. 1 (a) Clinical image of a mouse after 10 days of subcutaneous melanoma cell implantation, (b) procedure for LIBS sample preparation, and (c) optical image of the melanoma tissue section for LIBS elemental mapping.

a map showing the cancer and normal tissue regions. Although elemental mapping of solid samples by LIBS has been investigated by many researchers previously,^{13–16} LIBS elemental mapping of biological samples is relatively new. Recently, Motto-Ros et al. published a number of papers for LIBS imaging of biosamples. For example, Sancey et al.¹⁷ reported that the elements in mouse kidney embedded with Gd-based nanoparticles could be imaged with 10- μm resolution using a nanosecond (ns) 266 nm Nd:YAG laser-based LIBS. Also, Moncayo et al.¹⁸ took LIBS image of different types of paraffin embedded human tissue. Bonta et al.¹⁹ used LIBS for elemental mapping of human tumor in conjunction with laser ablation inductively coupled plasma mass spectrometry (LA-ICP-MS), where ns-LIBS was used for the mapping of major and minor elements while LA-ICP-MS was for trace elements. As shown in these studies, a nanosecond infrared or ultraviolet laser was commonly adopted in LIBS elemental mapping. However, a femtosecond-laser-based LIBS (fs-LIBS) can provide several advantages over ns-LIBS such as smaller heat-affected zone, lower ablation threshold, potentially finer spatial and depth resolution, and lower background emission.^{20–22} On the other hand, changes in sample condition, e.g., water content variation, can also affect the LIBS signal for biological samples.^{6,23} Therefore, for LIBS analysis of biological samples, it is desirable to perform the analysis under the conditions as close as possible to the original samples.

In this work, we report the results of fs-LIBS analysis and elemental mapping of cryosectioned melanoma sample as an imaging technique to differentiate the tumor and dermis regions. The sample was prepared by frozen tissue technique, the same procedure as in Mohs' surgery so that the LIBS elemental mapping image could be directly compared with the haematoxylin and eosin (H&E) staining image and evaluated for accuracy. It is shown that the skin cancer and dermis regions are clearly distinguished on the LIBS elemental mapping image and consistent with the histologically determined ones, demonstrating the feasibility of LIBS as a useful technique for faster determination of skin cancer regions.

2 Materials and Methods

2.1 Sample Preparation

For the preparation of melanoma sample for LIBS imaging, 1×10^6 B16/F10 cells, a well-known murine melanoma cell

line, in 100 μL of 0.9% NaCl solution were implanted in the back skin of 6 to 8 weeks old female SKH-1 mice. After 10 days from the implantation, melanoma lesions were developed on the mice as shown in Fig. 1(a). Then the skin tissues including both melanoma lesion and normal dermis were excised from the mice by a procedure shown in Fig. 1(b) for both LIBS elemental mapping and histologic analysis. For LIBS analysis, the excised tissue was first frozen and sectioned to 50- μm thickness using a cryostat (Cryocut 3000, Leica Biosystems, Nussloch, Germany) and then placed on a piece of silicon wafer for ablation. The frozen sectioning is a technique being used for histologic examination in Mohs surgery.²⁴ Figure 1(c) shows an optical image (50 \times ; SZ1145TRPT, Olympus Korea Co., Republic of Korea) of thereby produced tissue section over which LIBS elemental mapping was performed. The histology sample was also collected from the same excised tissue but was sectioned to 4- μm thick slices after fixing in 4% paraformaldehyde and embedding in paraffin, and stained with H&E.

Note that the sectioned LIBS sample and histology sample were not the same. Instead, they were collected from the same excised tissue within a few tens of micrometer thickness range. Therefore, it was assumed that the cancer profiles on the LIBS sample and histology sample were the same.

All procedures for sample preparation were approved by the Animal Care and Use Committee of Gwangju Institute of Science and Technology and performed in accordance with NIH guidelines (GIST-05).

2.2 LIBS Measurement

Figure 2 shows a schematic of the fs-LIBS set up used in this study. The ablation of sectioned tissue sample was carried out using a diode-pumped ytterbium femtosecond laser ($\lambda = 1030$ nm, $\tau = 550$ fs; s-pulse HP, amplitude systems). The laser beam was focused to a spot diameter of about 65 μm on the sample surface using an objective lens (magnification = 5 \times) and the laser pulse energy was set to 250 μJ , in which the corresponding laser fluence became about 7.42 J/cm^2 . On the laser spot, argon gas was injected in the direction of about 30 deg from the sample surface at the flow rate of 15 L/min for signal enhancement. Argon is often used as the buffer gas during LIBS experiments, mainly for signal enhancement. We used argon only during the measurement and the experiment was carried out in a well-ventilated environment. So there was little danger of asphyxiation.

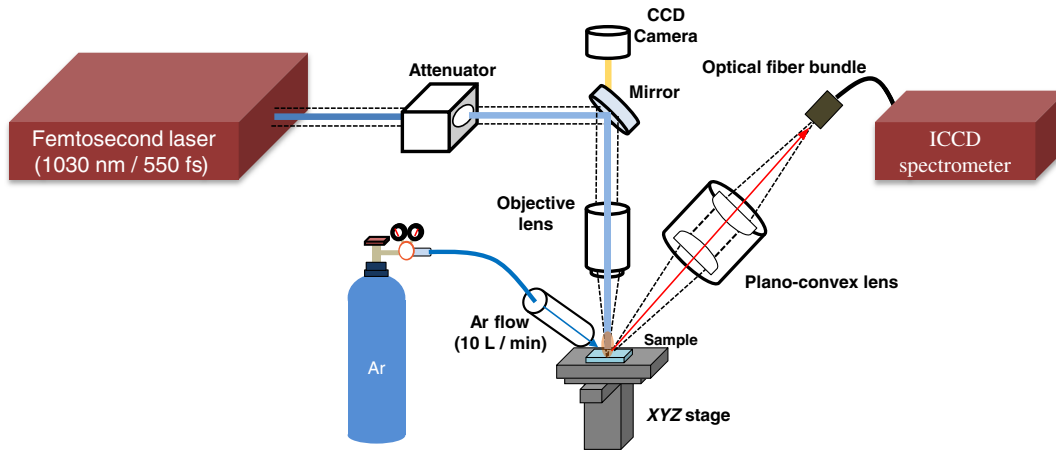


Fig. 2 Schematic diagram of the LIBS system.

An intensified charge coupled device (ICCD; PI-MAX3, Princeton Instruments, grating = 2400 grooves/mm, spectral width = ~ 60 nm, resolution = ~ 0.1 nm, and gain = 5) with high sensitivity was employed to detect the plasma emission because the emission intensity of LIBS plasma decreases rapidly at reduced spot diameter. The gate width of the ICCD spectrometer was set to $1 \mu\text{s}$ with $0.1 \mu\text{s}$ delay. Previously, we reported the LIBS data of melanoma and dermis measured using a nanosecond laser and a CCD spectrometer over a wide spectral range (200 to 900 nm).¹² The results showed that among the various detected elements (C, Mg, Ca, Na, H, O, N, and Cl), Mg and Ca showed significantly higher intensities in melanoma than in dermis, whereas other elements showed little difference. It was also shown that the Mg and Ca signals appeared at Mg (II) 279.553 nm, Mg (II) 280.170 nm, Ca (II) 393.366 nm, and Ca (II) 369.847 nm. The ICCD spectrometer used in this study had a limited spectral width (~ 60 nm), which could not cover the spectral regime including both elements. Thus either of the Mg or Ca peaks had to be measured in experiments, and we selected the Mg peak because it was well isolated and had low background.

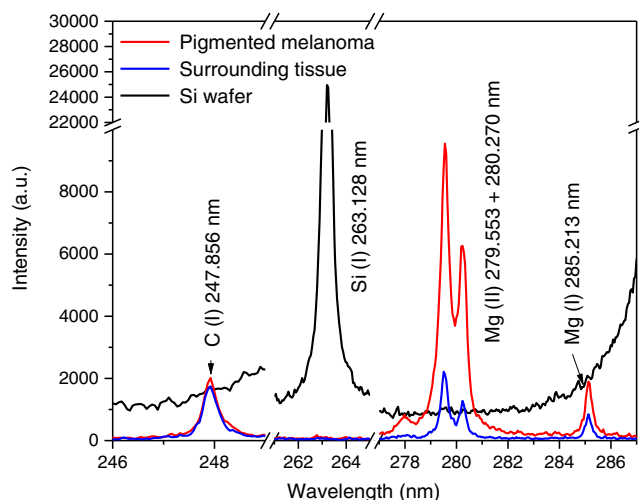


Fig. 3 Intensities of LIBS spectra measured from the pigmented melanoma, surrounding tissue, and Si wafer substrate.

3 Results

3.1 LIBS Signal Intensity

Figure 3 shows the LIBS spectra measured from the pigmented melanoma and the surrounding tissue of the sectioned ablation sample [see Fig. 1(c) for the LIBS measurement locations on the pigmented melanoma (red dot) and surrounding tissue (blue dot)]. It is seen that the intensity of the carbon peak, C(I) 247.856 nm, is nearly the same for both pigmented melanoma and surrounding tissue. This result is consistent with the earlier report that carbon content is independent of malignancy status of tissue.⁶ In contrast, the intensities of magnesium peaks, Mg(II) 279.553 + 280.270 nm and Mg(I) 285.213 nm, of the pigmented melanoma were found to be significantly higher than those in the surrounding tissue, which reconfirmed our previous results.¹² Note that the silicon peak Si(I) 236.128 nm, obtained by ablating a bear silicon wafer, is also shown in Fig. 3 in order to show that the measured carbon and magnesium signals were not interfered by the substrate.

3.2 Elemental Mapping

LIBS elemental mapping was performed by ablating the sectioned tissue on silicon wafer in Fig. 4(a) along a 25×25 spot array (total 625 spots). Since the laser spot diameter was about $65 \mu\text{m}$, the spot-to-spot distance was kept $70 \mu\text{m}$ during mapping so that no overlap between spots may have taken place. It took about 10 min to complete the mapping at the repetition rate of 1 Hz, but the mapping time may be reduced substantially by increasing the laser repetition rate.

The intensity of each spectral line in Fig. 3 was calculated by integrating the area under the peak using MATLAB. Also since the Mg(II) 279.553 nm and Mg(II) 280.270 nm lines are heavily overlapped and these lines have the same upper and lower level energies, the intensities of these lines were added and represented by a single value. Note that the intensities of spectral lines of an element having the same upper and lower level energies change with similar tendency during LIBS measurement.²⁵ Figures 4(b) and 4(c) show the LIBS elemental maps constructed with the C(I) 247.856 nm and Mg(II) 279.553 + 280.270 nm intensities, respectively, using Origin. It is clear from Fig. 4(b) that the intensity of C(I) 247.856 nm line is little or weakly influenced by the existence

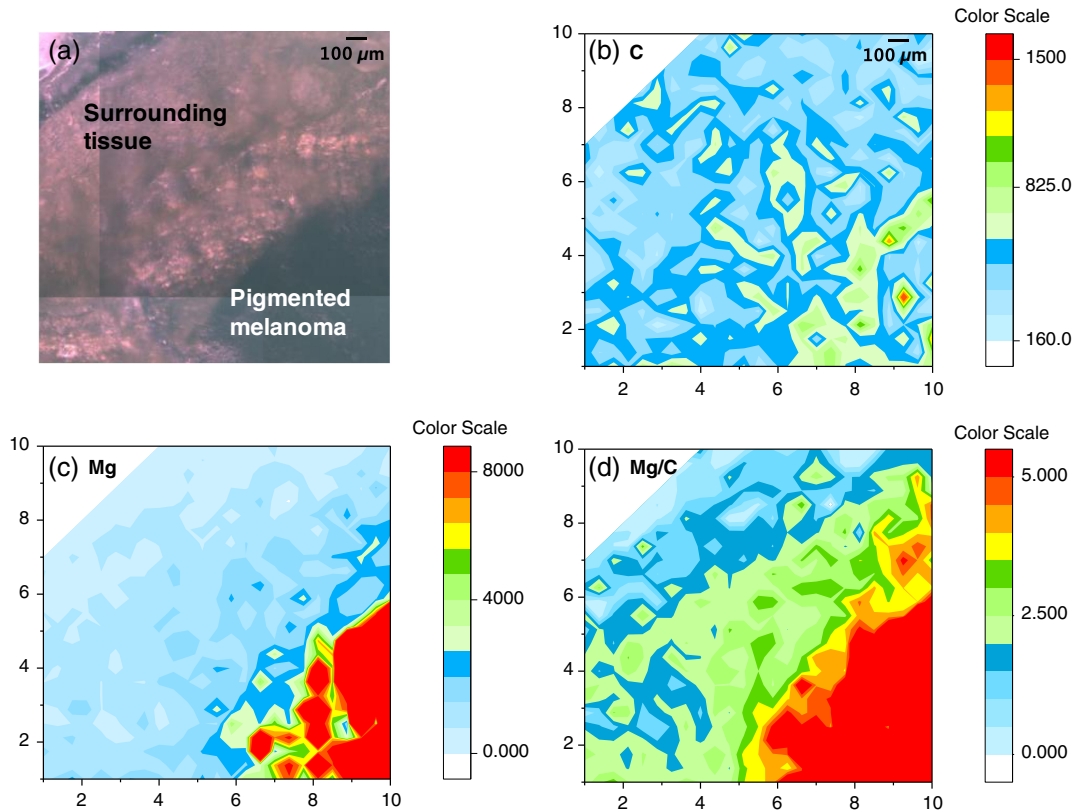


Fig. 4 (a) CCD image of the melanoma tissue section on silicon wafer before ablation, and the LIBS intensity maps of (b) C(I) 247.856 nm and (c) Mg(II) 279.553 + 280.270 nm lines, and (d) the map of Mg(II)/C(I) intensity ratio.

of melanoma, showing only a slight increase of intensity in the pigmented melanoma region. This result reconfirms that carbon concentration is hardly influenced by the cancer status of tissue. On the contrary, the intensity of Mg(II) 279.553 + 280.270 nm line in Fig. 4(c) shows a strong contrast between the pigmented melanoma region and the surrounding tissue. It is known that melanoma cells tend to infiltrate into the surrounding tissue. Considering the common existence of border region, in which isolated melanoma cells are frequently found, it is uncertain if the observed sharp contrast of Mg signal intensity in Fig. 4(c) reflects the actual variation of elemental concentration across the border of pigmented melanoma and surrounding tissue regions. In addition, the intensity of Mg(II) 279.553 + 280.270 nm line within the pigmented melanoma region appears nonuniform, which could be due to either true Mg concentration change or plasma fluctuation.

To reduce the possible variation of emission intensity due to plasma fluctuation, the intensity map was reconstructed by normalizing the Mg(II) 275.553 + 280.270 nm intensity by that of the C(I) 247.856 nm line. The resulting map in Fig. 4(d) shows a gradual decrease of normalized intensity, $I_{\text{Mg(II)} 279.553+280.270 \text{ nm}} / I_{\text{C(I)} 247.856 \text{ nm}}$, toward the surrounding tissue. The contours of the pigmented melanoma and the surrounding tissue in this elemental map, Fig. 4(d), seem to closely match the morphological features observed by the optical image in Fig. 4(a) [or that in Fig. 1(c)].

4 Discussion

To interpret the LIBS elemental mapping results, the intensity ratio map ($I_{\text{Mg}}/I_{\text{C}}$) in Fig. 4(d) was compared with the histology

image shown in Fig. 5. Again, note that the histology tissue section was not the same as the ablation tissue section, but the histology sample was collected from the same excised tissue within a few tens of micrometer thickness so that the observed features of melanoma may remain as close as possible between the sectioned histology sample and sectioned LIBS sample. The histologic features in Fig. 5 reveal mainly three different regimes, i.e., the pigmented melanoma, surrounding tissue locally containing nonpigmented melanoma cells (or mixed

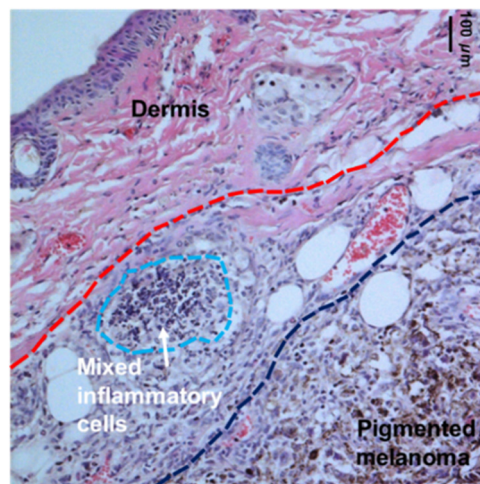


Fig. 5 Histologic features of the skin section showing pigmented melanoma, surrounding tissue containing nonpigmented melanoma cells, mixed inflammatory cells, and overlying dermis.

inflammatory cells), and normal dermis. The size and location of these three regimes appear to match the high-intensity region (shown in red color, $I_{Mg}/I_C = \sim 5$ to 100), medium intensity region (yellow and orange color, $I_{Mg}/I_C = \sim 3.5$ to 5; greenish color, $I_{Mg}/I_C = \sim 2$ to 3.5), and the low-intensity region (bluish color, $I_{Mg}/I_C < 2$) represented by the contours in the LIBS elemental map, Fig. 4(d). The I_{Mg}/I_C value over the elemental map shows a gradual decrease toward the dermis as expected. However, the location of tumor border is presumed to be near the light green and dark blue area on the basis of the histology image in Fig. 5 rather than the intensity ratio values. Note that the laser spot diameter in this study was about $65 \mu\text{m}$, which is much greater than the size of melanoma cells ranging from 10 to $30 \mu\text{m}$.²⁶ Therefore, the elemental mapping image in Fig. 4 cannot reflect the microscopic or cell-level variations of the cancer (e.g., pagetoid spread or small nests). Nonetheless, since the overall signal intensity within the melanoma cell containing areas is supposedly higher than that of dermis, it is considered that the variation of signal intensity still represents a meaningful information about cancer cell containing area. In principle, a further reduction of laser spot diameter close to cell size can be possible if a higher magnification focusing optics and a higher sensitivity detector are employed, allowing an elemental mapping at an improved spatial resolution.

In conjunction with the histology results, the variation of Mg (II)/C(I) intensity ratio over the LIBS elemental map in Fig. 4(d) may be explained by the role of Mg in metabolism. In general, melanoma has high cellular density as observed in Fig. 5 and shows active metabolism with robust protein biosynthesis. In addition to the melanoma cells, diverse forms of inflammatory cells observed between the pigmented melanoma and normal dermis also have active metabolism and produce a variety of enzymes.²⁷ On the other hand, Mg is known to be an essential component for protein biosynthesis^{28,29} and a cofactor of enzymes for general metabolic pathways and nucleic acid biochemistry.^{30,31} Thus compared with dermis which mainly consisted of collagen bundles and fibroblasts, the cell density and metabolic activity within the pigmented melanoma are expected to be significantly higher than those of dermis. Similarly, the cell density and metabolic activity would be high in the immediate vicinity of pigmented melanoma and drop gradually as approached the dermis. The intensity map of Mg(II)/C(I) in Fig. 4(d), which shows the highest Mg concentration in the pigmented melanoma region with a gradual decrease toward the surrounding tissue, is understood to reflect these differences in cell density and metabolic activity depending on the cancer status of tissue over these regions. On the contrary, the difference in pigment density between melanoma and dermis is considered to have little influence in the signal intensity change, because, in our previous study for LIBS analyses of melanoma with pellet and excised tissue samples, Mg intensity was found to be also higher in melanoma even after the absorption property difference between pigmented and nonpigmented regions was compensated by normalization.¹²

5 Conclusion

It is demonstrated that by fs-LIBS, a detailed elemental map showing the changes of LIBS signal intensity over melanoma and surrounding tissue could be established. The variation of normalized LIBS signal intensity over the melanoma and surrounding tissue closely matched the morphological and

histologic features of the lesion. The results in this study showed the potential of LIBS as a method to differentiate melanoma and dermis. Since the spatial resolution can be further improved with appropriate lasers and optics, it is considered that with clinical verification by more histologic comparison and other modalities, fs-LIBS mapping of melanoma can provide a realistic option for fast histologic interpretation of melanoma during micrographic surgery. Although this study was for LIBS analysis of melanoma cryostat sections, the same approach may be applicable for other types of skin cancer.

Disclosures

The authors declare that there are no conflicts of interest related to this article.

Acknowledgments

This work was supported by the National Research Foundation of Korea (NRF) grant funded by the Korea Government (MEST) (No. 2014049289).

References

1. C. Garbe et al., "Diagnosis and treatment of melanoma. European consensus-based interdisciplinary guideline—Update 2012," *Eur. J. Cancer* **48**(15), 2375–2390 (2012).
2. M. J. Sladden et al., "Surgical excision margins for primary cutaneous melanoma," *Cochrane Database of Syst. Rev.* (4), CD004835 (2009).
3. D. L. Shriner et al., "Mohs micrographic surgery," *J. Am. Acad. Dermatol.* **39**(1), 79–97 (1998).
4. J. M. Amici et al., "A prospective study of the incidence of complications associated with dermatological surgery," *Br. J. Dermatol.* **153**(5), 967–971 (2005).
5. A. Kumar et al., "Characterization of malignant tissue cells by laser-induced breakdown spectroscopy," *Appl. Opt.* **43**(28), 5399–5403 (2004).
6. A. El-Hussein et al., "Exploiting LIBS as a spectrochemical analytical technique in diagnosis of some types of human malignancies," *Talanta* **82**(2), 495–501 (2010).
7. F. Mehari et al., "Investigation of the differentiation of ex vivo nerve and fat tissues using laser-induced breakdown spectroscopy (LIBS): prospects for tissue-specific laser surgery," *J. Biophotonics* **9**(10), 1021–1032 (2016).
8. S. Sasazawa et al., "Optical-fiber-based laser-induced breakdown spectroscopy for detection of early caries," *J. Biomed. Opt.* **20**(6), 065002 (2015).
9. E. Ly et al., "Combination of FTIR spectral imaging and chemometrics for tumour detection from paraffin-embedded biopsies," *Analyst* **133**(2), 197–205 (2008).
10. A. Nijssen et al., "Discriminating basal cell carcinoma from its surrounding tissue by Raman," *J. Invest. Dermatol.* **119**(1), 64–69 (2002).
11. D. Prochazka et al., "Combination of laser-induced breakdown spectroscopy and Raman spectroscopy for multivariate classification of bacteria," *Spectrochim. Acta, Part B* **139**, 6–12 (2018).
12. J. H. Han et al., "Differentiation of cutaneous melanoma from surrounding skin using laser-induced breakdown spectroscopy," *Biomed. Opt. Express* **7**(1), 57–66 (2016).
13. H. Bette and R. Noll, "High speed laser-induced breakdown spectrometry for scanning microanalysis," *J. Phys. Appl. Phys.* **37**, 1281–1288 (2004).
14. Q. L. Ma et al., "Multi-elemental mapping of a speleothem using laser-induced breakdown spectroscopy," *Spectrochim. Acta, Part B* **65**(8), 707–714 (2010).
15. D. Menut et al., "Micro-laser-induced breakdown spectroscopy technique: a powerful method for performing quantitative surface mapping on conductive and nonconductive samples," *Appl. Opt.* **42**(30), 6063–6071 (2003).
16. Z. Wang et al., "Application of laser-induced breakdown spectroscopy to real-time elemental monitoring of iron and steel making processes," *ISIJ Int.* **56**, 723–735 (2016).

17. L. Sancey et al., "Laser spectrometry for multi-elemental imaging of biological tissues," *Sci. Rep.* **4**, 6065 (2014).
18. S. Moncayo et al., "Multi-elemental imaging of paraffin-embedded human samples by laser-induced breakdown spectroscopy," *Spectrochim. Acta, Part B* **133**(1), 40–44 (2017).
19. M. Bonta et al., "Elemental mapping of biological samples by the combined use of LIBS and LA-ICP-MS," *J. Anal. At. Spectrom.* **31**, 252–258 (2016).
20. D. Santos et al., "Evaluation of femtosecond laser-induced breakdown spectroscopy for analysis of animal tissues," *Appl. Spectrosc.* **62**(10), 1137–1143 (2008).
21. R. K. Gill et al., "Characterization of femtosecond laser-induced breakdown spectroscopy (fsLIBS) and applications for biological samples," *Appl. Spectrosc.* **68**, 949–954 (2014).
22. H. Hou et al., "Three-dimensional elemental imaging of Li-ion solid-state electrolytes using fs-laser induced breakdown spectroscopy (LIBS)," *J. Anal. At. Spectrom.* **30**, 2295–2302 (2015).
23. Y. Moon et al., "Influence of water content on the laser-induced breakdown spectroscopy analysis of human cell pellet," *Spectrochim. Acta, Part B* **114**, 27–33 (2015).
24. O. Bakhtar et al., "Tissue preparation for MOHs' frozen sections: a comparison of three techniques," *Virchows Arch.* **450**(5), 513–518 (2007).
25. N. B. Zorov et al., "A review of normalization techniques in analytical atomic spectrometry with laser sampling: from single to multivariate correction," *Spectrochim. Acta, Part B* **65**(8), 642–657 (2010).
26. Y. Wang et al., "Fiber-laser-based photoacoustic microscopy and melanoma cell detection," *J. Biomed. Opt.* **16**(1), 011014 (2011).
27. L. M. Coussens and Z. Werb, "Inflammation and cancer," *Nature* **420**, 860–867 (2002).
28. C. Cillo et al., "Generation of drug-resistant variants in metastatic B16 mouse melanoma cell lines," *Cancer Res.* **47**(10), 2604–2608 (1987).
29. M. Terasaki and H. Rubin, "Evidence that intracellular magnesium is present in cells at a regulatory concentration for protein synthesis," *Proc. Natl. Acad. Sci. U. S. A.* **82**(21), 7324–7326 (1985).
30. J. A. Cowan, *The Biological Chemistry of Magnesium*, John Wiley & Sons, Ltd, New York (1995).
31. D. E. Wilcox, "Binuclear metallohydrolases," *Chem. Rev.* **96**(7), 2435–2458 (1996).

Youngmin Moon received his PhD in medical system engineering at the Gwangju Institute of Science and Technology in 2016. He is a postdoctoral researcher at Gwangju Institute of Science and Technology, Republic of Korea. His research interests include

elements analysis of biological tissues based on laser-induced breakdown spectroscopy, and development of low-power laser system for invasive therapy.

Jung Hyun Han received his PhD in medical system engineering from Gwangju Institute of Science and Technology. He is a graduate of Chonnam National University Medical School. He completed residency in the Department of Dermatology of Chonnam National University Hospital, Republic of Korea. His research interest includes the clinical dermatology, natural photoluminescence compounds, subcutaneous implantable device, laser-induced breakdown spectroscopy, and spectroscopic analysis in medical field.

Jang-hee Choi received his BS and MS degrees in physics from Chungnam National University in 2010 and 2013, respectively. He is a PhD candidate in mechanical engineering at Gwangju Institute of Science and Technology, Republic of Korea. His research focus on elemental analysis of solid and biological tissues based on laser-induced breakdown spectroscopy.

Sungho Shin received his BS degree in biomedical engineering from Yonsei University in 2012 and his MS degree in medical system engineering from Gwangju Institute of Science and Technology in 2014. He is a PhD candidate in mechanical engineering at the Gwangju Institute of Science and Technology, Republic of Korea. His research focuses on laser-tissue interaction mechanisms with low- and high-power laser and ongoing research includes application of laser-induced breakdown spectroscopy.

Yong-Chul Kim is a faculty member of the School of Life Sciences, Gwangju Institute of Science and Technology, Republic of Korea. He has worked in the field of medicinal chemistry for drug discovery for more than 20 years in NIH, University of Alabama at Birmingham, ChemBridge, Inc. and GIST, performing synthetic organic and combinatorial chemistry of the lead compounds from structure-based drug design for the optimization toward new drug candidates.

Sungho Jeong received his PhD in mechanical engineering from the University of California at Berkeley in 1997 and worked at Lawrence Berkeley National Laboratory during his doctoral and postdoctoral studies. He is a professor at Gwangju Institute of Science and Technology, Republic of Korea. His research focuses on laser ablation phenomena and their applications, and ongoing research includes application of laser-induced breakdown spectroscopy, laser materials processing, and laser interaction with biomedical materials.